Journal of Catalysis **212,** 63–75 (2002)
doi:10.1006/jcat.2002.3780

Hydrogenation of Toluene over Supported Pt and Pd Catalysts: Influence of Structural Factors on the Sulfur Tolerance

K. Thomas,[1] C. Binet, T. Chevreau, D. Cornet, and J.-P. Gilson

Laboratoire de Catalyse et Spectrochimie, ISMRA-CNRS-Université de Caen, 6, bd. du Maréchal Juin, 14050 Caen, France

Received April 29, 2002; revised July 29, 2002; accepted July 31, 2002

Pt, Pd, and PtPd metallic precursors are deposited on dealuminated FAU zeolites and on one amorphous silica–alumina. The catalytic activity is measured in the hydrogenation of toluene at 30 MPa total pressure, either in the absence or in the presence of sulfur (200 ppm in toluene). In the absence of sulfur, alloying Pt with Pd decreases the hydrogenation activity. In general, catalysts made from ammoniated precursors are the most active, with one remarkable exception. In the presence of sulfur, thioresistance is a function of reaction temperature, i.e., sulfur coverage of the metallic phase. Pd increases substantially the sulfur tolerance. The effect of support acidity on S tolerance is observed only at high sulfur coverage.

Key Words: **Pt; Pd; zeolite; silica–alumina; toluene, sulfur tolerance.**

INTRODUCTION

At the 2005 horizon, more-stringent regulations on the aromatics and sulfur levels of diesel fuels (<30 ppm of S and 3–5 wt% polynuclear aromatics) will further affect the refining industry, first in the U.S. and Europe. It is likely these regulations will also spread to all other areas of the world. Other petroleum fractions will also come under scrutiny. Refiners will have to respond by adding to the classical hydrodesulfurization catalysts more hydrogenating power. As a consequence, they will have to rely on noble metal-based catalysts (1) in hydrotreating reactions (HDS and hydrodearomatization). These catalysts will have to tolerate the residual sulfur present in the second reactor of a two-stage unit. PtPd catalysts supported on acidic carriers are already used commercially in niche markets like the so-called "City Diesel" sold in Sweden (2). Much work (3, 4) has already been done on various aspects of the catalyst design. The sulfur tolerance is often related to the electron density of the metallic clusters deposited on a support. However, the relative roles of the (bi)metallic phase and the acidic support are poorly understood. For instance, the effect of alloying another metal with Pt has been studied on an Al_2O_3 carrier (3), amorphous silica–alumina (5, 6), and zeolites (2, 7), while the effect of various acidic zeolites has also been examined (4).

The aim of this work is to determine which factors are the most important in the design of a sulfur tolerant catalyst. We elected to study catalysts representative of the commercial ones, i.e., containing low levels of Pt and/or Pd (0.3 and 0.5 wt%, respectively) on supports with carefully controlled acidity (8). A series of dealuminated FAU zeolites and one amorphous silica–alumina were selected as supports. Catalysts with various acidities and metallic functions were prepared by impregnation with ammine or chloride metal precursors. Acidity was characterized by FT-IR spectroscopy, and the metallic phase by CO adsorption monitored by FT-IR spectroscopy. The effects of the metal function, support acidity, and precursor used for impregnation were evaluated in toluene hydrogenation: first in the absence, then in the presence of 200 ppm H_2S. The laboratory-prepared catalysts have also been compared with three industrial catalysts.

EXPERIMENTAL

Catalysts

A first series of laboratory-prepared catalysts was based on commercial faujasites (CBV from PQ Corp.) commonly used in manufacturing bimetallic PtPd catalyst (8–10), and consisting of Y zeolites steamed at various temperatures. The CBV-500, with an overall Si/Al = 2.8, was not acid washed. Acid treated samples were also used: their overall Si/Al ratios of 22 (CBV-740), 39 (CBV-760), and 40 (CBV-780) were measured by chemical analysis. BET areas ranged from 872 (CBV-500) to 937 $m^2\ g^{-1}$ (CBV-780).

Another series of catalysts was prepared from an amorphous silica–alumina, the S5A support from Grace Davison, with Si/Al = 5, BET area = 380 $m^2\ g^{-1}$, and pore volume = 1.08 $cm^3\ g^{-1}$.

The support powders were impregnated by the incipient wetness technique, using aqueous solutions containing the Pt/Pd ions and an excess of nitric acid such that the ratio NO_3^-/metal was 20 mol/mol. Final metal contents were

[1] To whom correspondence should be addressed. Fax: +32 2 31 45 28 22. E-mail: karine.thomas@ismra.fr.

0021-9517/02 $35.00

close to 0.3 wt% Pt, or 0.5% Pd, or (0.3% Pt + 0.5% Pd). Solutions of the ammine complexes $Pt(NH_3)_4(NO_3)_2$, $Pd((NH_3)_4(NO_3)_2$, or both were used to prepare the catalysts referred to as "am." For the "Cl" catalysts, the solution contained H_2PtCl_6 or $PdCl_2$, or both. The impregnated solids were oven dried, then carefully calcined under a gas flow containing 2% O_2 in N_2 (flow rate, 6 ml/g-cat min^{-1}) while temperature was slowly raised from 300 to 573 K at a rate of 0.5 K min^{-1}. Reduction with hydrogen was performed at 573 K in the catalytic reactor, prior the activity test (flow rate, 3300 ml/g-cat min^{-1}).

Three industrial catalysts (I_1, I_2, I_3) available as extrudates were also tested. Catalysts I_1 and I_2 had surface areas of 399 and 574 m^2 g^{-1}, respectively, and contained zeolitic material. Catalyst I_3, with a surface area of 395 m^2 g^{-1}, used a silica–alumina carrier. The metal loadings were about 0.85 wt% (Pt + Pd) for I_1 and I_2, and 1.1% for I_3.

Catalytic Tests

Hydrogenation of toluene was carried out under 3 MPa total pressure in a flow reactor made of stainless steel. A fixed catalytic bed was placed in a quartz tube fitting the inside wall of the reactor. The bed, about 10 mm long and 9 mm in diameter, was made of $W = 0.03$ g catalyst powder in most experiments without sulfur ($W = 0.06$ g with sulfur), diluted with an equal mass of silicon carbide with similar granulometry. The industrial catalysts were ground to particles with size 0.3–0.5 mm and also mixed with SiC. The whole reactor system was thermostated at 353 K to avoid any condensation.

Toluene was delivered through a liquid chromatography pump (Gilson 302) at a rate of 0.3 ml per h, then it vaporized in the hydrogen flow (7.8 liter per h). The toluene partial pressure P_0 at the reactor entry was thus 25 kPa (188 Torr), and the "contact time" $W/F = 0.011$ kg h mol^{-1} in most cases. Experiments involving sulfur were performed by adding a small amount of dimethyldisulfide (240 μl DMDS per liter, i.e., 200 ppm S in solution) to toluene. DMDS was fully converted into H_2S and methane, and the H_2S partial pressure in the reactor was about 13 Pa. In such cases, the contact time was $W/F = 0.022$ kg h mol^{-1}. Gaseous samples of the reacted products were collected at atmospheric pressure and analyzed online with a gas chromatograph equipped with a PLOT column (fused silica Al_2O_3–KCl). It was verified that the reactions were not limited by external or internal diffusion.

IR Spectroscopy

IR spectra were recorded on a Nicolet 710 instrument and processed with the Omnic and Peaksolve software. Unreduced catalysts and supports were compressed in self-supported thin wafers (10–20 mg), then placed in a gas handling system connected to the spectrometer cell. All adsorbates were previously dried in a liquid nitrogen trap.

The accessibility of supported metals was determined with the CO probe technique (11). Known amounts of carbon monoxide (Air Liquide) were adsorbed at room temperature over the catalysts that were previously reduced by H_2 at 573 K (three doses at 13.3-kPa pressure).

Densities of acid sites were estimated by pyridine adsorption (Fluka purum) at 393 K and $P = 67$ Pa. The samples were then evacuated at 393 K and cooled to room temperature to record IR spectra. Acid strengths were evaluated with CO adsorbed at 100 K. A dedicated homemade low-temperature cell was used in these experiments.

RESULTS

Toluene Hydrogenation without Sulfur

The bimetallic (PtPd) catalysts and some monometallic (Pt or Pd) catalysts were first evaluated for the hydrogenation of toluene with a sulfur-free feed. Methylcyclohexane was the only product, and the full range of conversion levels could be reached between 333 and 433 K. Generally, the activity decreased by less than 0.5% during the first 2 h on stream, then remained stable at least for 24 h. Conversions of toluene measured at several temperatures but at fixed contact time over catalysts supported on zeolite CBV-780 are plotted in Fig. 1. They depend considerably on the metal and the precursor. Further data were recorded at other contact times with different catalyst masses.

In order to derive kinetic parameters from data gathered in such a way, a kinetic model is needed. The rates of toluene hydrogenation measured at low conversion levels and below 423 K are reported to be zero order in aromatic

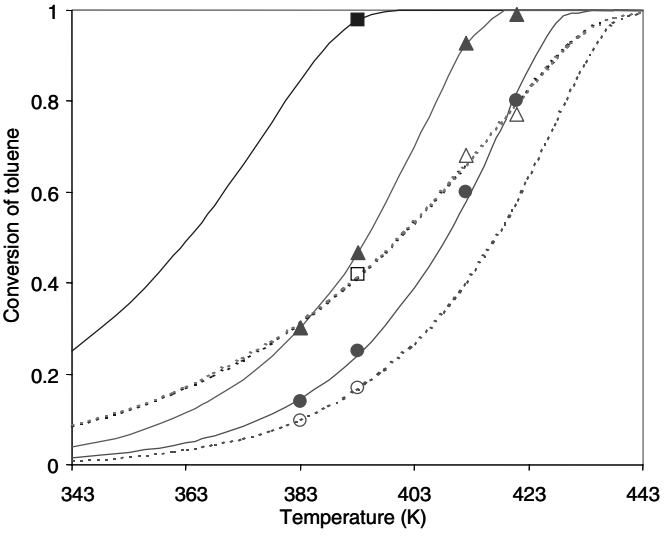

FIG. 1. Hydrogenation of toluene over catalysts supported on CBV-780: conversion versus temperature at $W/F = 0.011$ kg h mol^{-1}; $P(H_2) = 3$ MPa; $P_0(tol) = 24$ kPa. No sulfur. (Solid lines) am precursors: ■, Pt (0.3%); ●, Pd (0.5%); ▲, Pt (0.3%) + Pd (0.5%). (Dashed lines) Cl precursors: □, Pt (0.3%); ○, Pd (0.5%); △, Pt (0.3) + Pd (0.5%).

pressure (12–15). This point was easily checked with one of our catalysts by simply changing the hydrogen flow rate at 393 K: the conversion remained stable at $22.8 \pm 0.5\%$ as the toluene partial pressure varied from 24 to 44 kPa. However, a zero-order rate law cannot be used in a wide range of conversion levels, especially with the most active solids. Results were better represented with a Langmuir–Hinshelwood rate equation; i.e.,

$$r(\text{mol h}^{-1}\,\text{kg}^{-1}) = \frac{kbP_{\text{tol}}}{1 + bP_{\text{tol}}},$$

where P_{tol} (Pa) is the toluene pressure (P_0 at entrance) and b (Pa^{-1}) an adsorptionlike coefficient; the rate constant k (mol h^{-1} kg^{-1}) varies with an activation energy E_a.

The conversion data were fitted with curves calculated using this rate equation (Fig. 1). The bP_0 values were found close to 10 for the CBV-780 catalysts, as well as for those using other supports. Parameter b could not be accurately determined, as the reactor slightly deviated from uniform plug flow, which may cause errors at high conversion levels. However, b appeared nearly constant with temperature. Therefore, each catalyst could be characterized by the initial rate $r_0 = kbP_0/(1 + bP_0)$ calculated at 393 K, and the activation energy E_a. Table 1 reports the r_0 and E_a for the CBV-780 catalysts, and the r_0 values are pictured in Fig. 2. From these, a turnover frequency may be deduced ("TOF" = moles converted per mole-accessible metal and per hour), as explained later.

Among the CBV-780 catalysts, those containing Pt only display higher initial rates and lower activation energies than those containing Pd or Pt–Pd. With the "am" precursor, for instance, r_0 for the Pt_{am}/CBV-780 is about fives times that of the corresponding Pd_{am} catalyst, with E_a values equal to 36 and 64 kJ mol^{-1}, respectively. The higher hydrogenation capacity of platinum is more obvious when considering the rates per mole of total metal: then the intrinsic activity of Pt is 15.5 times that of Pd. Catalysts made with chloride precursors are distinctly less active than their

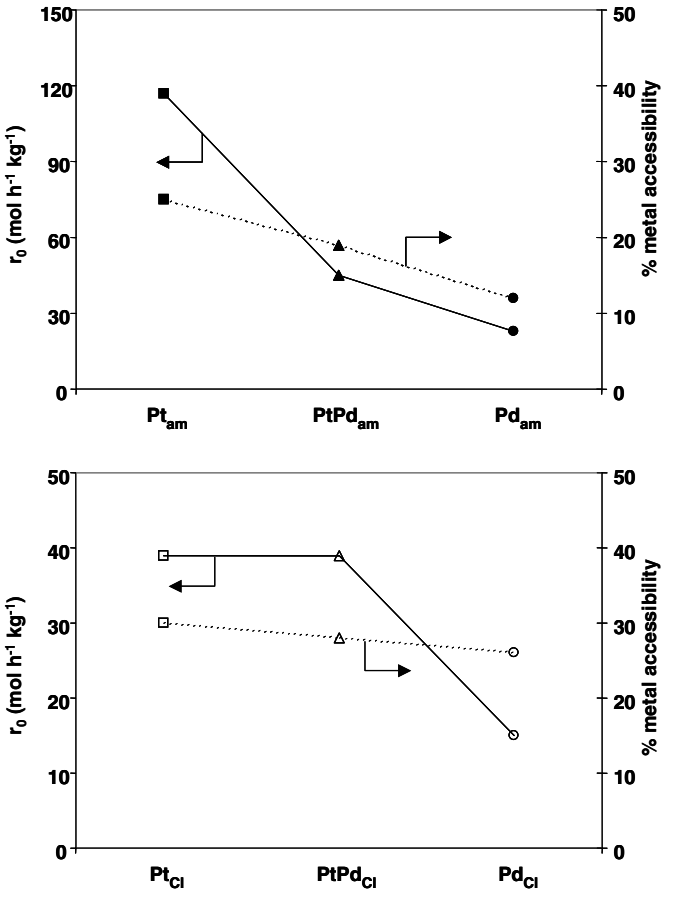

FIG. 2. Rates of hydrogenation r_0 (no sulfur) and metal accessibilities Acc (measured by CO adsorption) for catalysts supported on CBV-780. (Upper graph) am precursor; (lower graph) Cl precursor.

TABLE 1

Hydrogenation of Toluene over Catalysts Based on Zeolite CBV-780: Kinetic Data for the Reaction without Sulfur

Metal	Precursor	bP_o	E_a (kJ mol^{-1})	r_o at 393 K (mol h^{-1} kg^{-1})	Metal accessibility (%)	TOF at 393 K (s^{-1})
Pt	Am	9	36	117	25	8.44
Pd	Am	10	64	23	12	1.11
PtPd	Am	10	57	45	19	1.06
Pt	Cl	9	36	39	30	2.36
Pd	Cl	9	64	15	26	0.33
PtPd	Cl	9	36	39	28	0.62

Note. Measurements performed at $P(H_2) = 3$ MPa and $P_0(\text{Tol}) = 24$ kPa.

am analogs: the initial rate, r_0, for Pt is only 2.6 times that of Pd. Nevertheless, similar activation energies were found for Cl and am samples.

The bimetallic PtPd/CBV-780 catalysts exhibit higher initial rates r_0 and lower activation energies E_a than the Pd ones, whatever the precursor. With the am precursor, the PtPd has a lower r_0 and higher E_a than the Pt, but with the Cl precursor the PtPd and Pt have nearly the same r_0 and E_a. As the loading in the bimetallic catalysts is the sum of that in the monometallic Pt and Pd, these data suggest that the PtPd catalyst is not simply made of two distinct Pt and Pd phases. Therefore, the catalytic activity in the CBV-780 series mainly depends on the nature of the metal, but the type of metal precursor has also some importance.

The influence of the carrier was then considered. Conversions measured over catalysts supported on the other zeolites, on silica–alumina, and on the industrial catalysts were treated as above, and the results are gathered in Table 2. The initial rates at 393 K as well as activation energies vary somewhat with the support. For the bimetallic $PtPd_{am}$ catalysts, supports CBV-780 and CBV-760 appear

TABLE 2

Initial Rates of Hydrogenation (Reaction without Sulfur) and Metal Accessibilities for Catalysts Based on Other Zeolites or Silica–Alumina, and for Industrial Catalysts

Support	Metal	E_a (kJ mol^{-1})	r_o at 393 K (mol h^{-1} kg^{-1})	Accessibility (%)	TOF at 393 K (s^{-1})
CBV-760	$PtPd_{am}$	37	45	20	1
CBV-740	$PtPd_{am}$	63	32	20	0.73
	$PtPd_{Cl}$	54	30	18	0.75
CBV-500	$PtPd_{am}$	72	6	18	0.14
S5A	Pt_{am}	64	35	28	2.25
	Pd_{am}	68	24	13	1.09
	$PtPd_{am}$	58	26	15	0.78
	Pt_{Cl}	73	10	—	—
	Pd_{Cl}	65	11	—	—
	$PtPd_{Cl}$	69	15	20	0.33
I_1	PtPd	48	24	17	0.58
I_2	PtPd	38	29	40	0.30
I_3	PtPd	64	15	28	0.17

equivalent, while CBV-740 is slightly inferior. For catalyst $PtPd_{am}$/CBV-500 the activity is particularly low and the activation energy quite high. However, this catalyst is peculiar, since it deactivated much more strongly than any other during the initial period.

Among catalysts using the ASA support, those made with the am precursor are slightly less active than their zeolite analogs, as judged from the r_0 values. Again the ammine precursor appears more efficient than the chloride, and differences in activities are larger than with the zeolite supports. Furthermore, activation energies for the ASA catalysts are generally higher than for the zeolite catalysts. Finally, the rates for the three industrial catalysts are well in line with the laboratory-made ones, with a remarkably small activation energy for sample I_2.

As many factors are involved, more information on the catalyst structure is needed. The nature and the dispersion (accessibility) of the metal phase will now be examined by means of IR.

Accessibility of the Metal

When increments of CO (2×10^{-6} mol per g catalyst) were introduced at room temperature over the reduced catalysts, absorption bands due to Pt–CO or Pd–CO species appeared in the IR spectrum, at wavenumbers from 2100 to 1700 cm^{-1} (16–19). Their overall intensity increased at first with the ratio ρ (moles of CO adsorbed/mole of total metal), then remained stable on further adsorption. The change in slope occurred at a residual CO pressure less than 50 Pa. The accessibility (Acc) of the metal may be deduced from the ρ value at incipient saturation if the adsorption stoichiometry is known. In previous studies the number of CO bound to one exposed metal atom was found to vary somewhat with the metal and the crystallite size (20–22). For palladium, a one-to-one stoichiometry was found by Binet *et al.* (11) whatever the crystalline face exposed. The same ratio was tentatively assumed to compare the Pt and PtPd catalysts.

Accessibilities measured for metals supported on zeolite CBV-780 are shown in Fig. 2 and Table 1. In the Pt_{am} catalyst, for instance, 25% of the metal is found to be accessible. This is well under the 85% dispersion reported for some ultradispersed Pt/Al_2O_3 reforming catalysts (23), but not far from those reported for Pt/H–beta (24). Although the dispersion of Pt_{am}/CBV-780 appears far from 100%, the other metals loaded on the same support present lower accessibilities, 12% for the Pd_{am} and 19% for the bimetallic $PtPd_{am}$ (Fig. 2). Catalysts impregnated with the Cl precursor gave more homogeneous and slightly better accessibilities, 26 and 28%, respectively, for monometallic and bimetallic catalysts.

Results for the other catalysts of this study are reported in Table 2. The PtPd supported on zeolites CBV-760, CBV-740, and CBV-500 have accessibilities between 18 and 20% and compare well to that for $PtPd_{am}$/CBV-780. For catalysts using the silica–alumina carrier, complete data were obtained for the am precursor only. Metal accessibilities are only slightly under those with the zeolite supports, except for the Pt_{am} catalyst, despite a much lower surface area (390 versus 940 m^2 g^{-1}). The Acc values follow the same trend as with CBV-780; i.e., Pt > PtPd > Pd. Finally, the Acc for the industrial catalysts are in line with the preceding ones, except for sample I_2, whose dispersion appears better than any other.

Thus in the whole series of catalysts, the accessibilities of Pt, Pd, or PtPd do not depend markedly on either the support or the precursor, while turnover frequencies are seen to vary with both. For instance, the iso-dispersed $PtPd_{am}$ supported on CBV-780, CBV-760, and CBV-740 have different catalytic activities. Regarding the precursor effect, the PtPd catalysts supported on CBV-780 and S5A present a higher metal accessibility when they are prepared with Cl rather than with am precursor. Yet the reverse trend is observed for the activities. Therefore, differences in activity should be ascribed to properties of the metallic phases. More information on the exposed metal atoms is required and may be obtained from the IR spectra of adsorbed CO.

The State of Exposed Metal Atoms

In the IR spectra recorded on adsorption of CO at room temperature, various Me–CO species may be identified; they are characteristic of the exposed metal atoms. Detailed results will be presented only for the am catalysts supported on zeolite CBV-780. Fig. 3 shows the spectra recorded over Pt (3a), Pd (3b), and PtPd (3c) at a residual CO pressure of

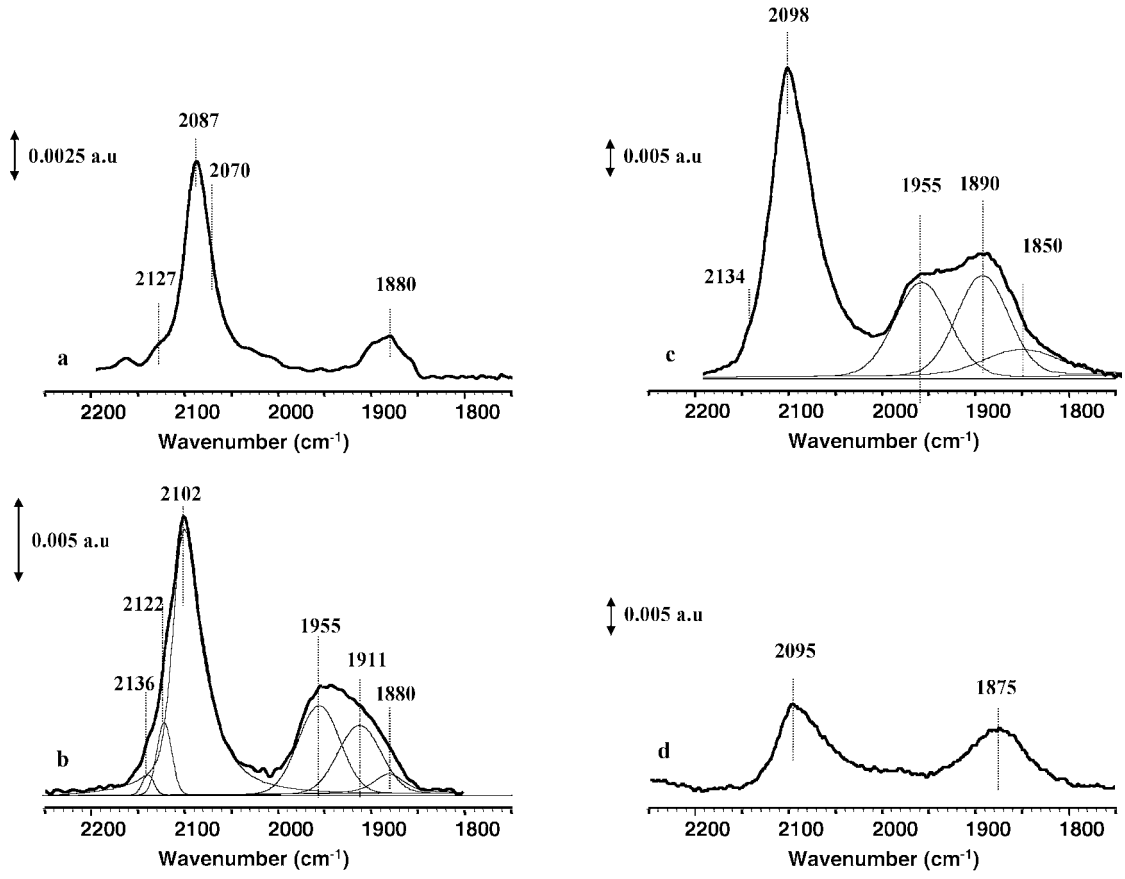

FIG. 3. Chemisorption of CO (298 K; $P_{CO} = 133$ Pa) over reduced metal catalysts supported on CBV-780. Infrared spectra in the ν(CO) region. (a) Pt_{am}; (b) Pd_{am}; (c) $PtPd_{am}$; (d) alloy (see text).

133 Pa, i.e., at saturation. The ν(CO) band near 2100 cm^{-1} arises from linear Me–CO species, while the complex signal below 2000 cm^{-1} is assigned to bridged CO entities.

In the bands recorded over the monometallic catalysts (Table 3), several components may be recognized by comparison with literature data obtained at similar CO coverage. Linear Me–CO species mainly occur on zerovalent Pt or Pd located on terraces or edges of metal particles, but a small number involve unreduced metal ions. The wavenumbers of the metal-bound CO species are higher for Pd than

TABLE 3

Adsorption of CO over Metals Supported on Zeolite CBV-780 ($T = 298$ K; $P_{CO} = 133$ Pa)

	Linear CO			Bridged CO		
Catalyst	$\bar{\nu}$ (max)	Components	Ref.	$\bar{\nu}$ (max)	Components	Ref.
Pt_{am}	2087: 2127(sh)	Oxidized Pt	25	1880	$Pt_2(CO)$	26
	2087	Pt terraces				
	2070	Pt edges				
Pd_{am}	2102: 2136, 2122	Oxidized Pd,	11, 27	1950: 1955 (B)	$Pd_2(CO)$ on (100)	11, 17, 28
	2102 (A)	Pd terraces or discontinuities		1911 (C)	$Pd_2(CO)$ on (111)	
				1880 (D)	$Pd_3(CO)$ on (111)	
$PtPd_{am}$	2098: 2134 (sh)	Oxidized Pt or Pd		1955 (B)	as for Pd	
	2102	Pd(CO)		1890: 1890 (C)		
	[2095]	[alloy]		[1875]	[alloy]	
	2087	Pt(CO)		1850 (D)		

Note. Summary of IR data in the ν(CO) region. Wavenumbers $\bar{\nu}$ are in cm^{-1}. Underlined values refer to absorption maxima, and bracketed values to new bands attributed to a PtPd alloy.

for Pt, and such high $\bar{\nu}$ give evidence for some interaction between the metal and the acidic support (25). The bands of bridged CO reveal adsorption on larger metallic areas. Three species may be distinguished over Pd (Table 3): they are designated as in (22). The high intensity of the bridged CO bands (B, C, D) may be related to the low metal dispersion. As one surface metal atom may be linked to more than one bridging CO, the relative importance of the linear and bridged CO signals may be reconciled with an overall Me/CO ratio equal to 1. When the CO gas was pumped off from the Pt catalyst, the intensity of the IR spectrum was little affected, but for the Pd and PtPd catalysts the decrease was important. In any case, the bands shifted to lower wavenumbers, showing weaker lateral interactions between adsorbed CO.

The spectrum recorded for the PtPd sample (Fig. 3c) is broadly similar to that of Pd. A similar observation was reported by Kazansky and co-workers for catalysts supported on NaY (29). The band of linear CO lies at 2098 cm^{-1} and its intensity decreases by 40% on evacuation, versus 84% for the Pd catalyst. This feature means that some CO is linearly adsorbed on Pd terraces. As the residual signal cannot arise from CO adsorbed only on Pt crystallites, it reveals the presence of mixed Pt–Pd zones. In XPS and EXAFS studies of supported PtPd catalysts, the formation of an alloy has been evidenced, but in most cases there is a strong tendency toward surface segregation of Pd (3, 30, 31). Furthermore, the IR band due to bridged species (below 2000 cm^{-1}) clearly exhibits two maxima. The spectrum cannot be reproduced by simply adding the monometallic spectra a and b (Fig. 3), even if weight factors are included to account for differences in metal accessibilities. However, in the PtPd whole spectrum, the contributions from the monometallics could be subtracted by adjusting the weight factors so as to reproduce the intensity of the B band at 1955 cm^{-1} (contribution of Pd only), and then suppress the shoulder at 2087 cm^{-1} (linear Pt–CO). The resulting spectrum c—$(0.1 \times a) - (1.3 \times b)$—appears as spectrum d in Fig. 3. Two new bands show up, the first one (2095 cm^{-1}) attributed to CO linearly adsorbed on Pt atoms adjacent to Pd, and the second one (1875 cm^{-1}) attributed to CO bridging mixed PtPd sites. Such an interpretation is consistent with the activity data, as the rate of hydrogenation on PtPd was found to be lower than on Pt. However, activation energies over bimetallic catalysts are lower than those for the Pd catalysts. This behavior could agree with a single metallic phase accommodating all of the Pt and Pd, or with a polyphase model where pure Pd crystallites coexist with mixed PtPd with nearly equivalent amounts of Pt and Pd. In the latter, the two metals interact strongly, while pure Pt zones are scarce.

Adsorption of CO over the bimetallic PtPd/CBV-780 prepared from the chlorinated precursors reveals the same features, and the presence of an alloy is also inferred. The main difference with these precursors lies in an incomplete reduction of the metals, due to the presence of residual chlorine on the surface (32). Again essentially similar results were found with the other zeolite supports. Finally, the spectra recorded for CO adsorbed on $PtPd_{am}$/ASA differed from the preceding ones only in the region of the bridging species. Two different bands were found for CO bridge bonded on Pd(100) faces, showing a greater heterogeneity in crystallite size with this support. Nevertheless, the same conclusions may be drawn as for the zeolites concerning the occurrence of an alloy.

Acidity of the Supports: Adsorption of Pyridine

The enhancement of the hydrogenation activity of metals due to the support acidity is well documented. It occurs both in the absence (12, 13, 33–35) and in the presence of sulfur (36, 37). Accordingly, the surface acidity of our samples was evaluated by IR, using two probe molecules with different selectivities.

The spectra of the bare supports in the ν(OH) region are displayed in Fig. 4a. The three steamed FAU zeolites

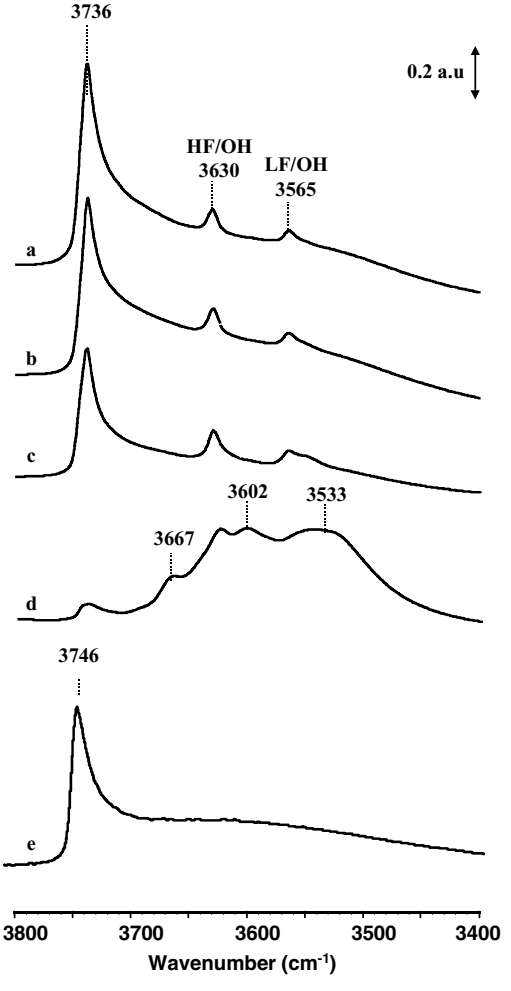

FIG. 4. IR spectra in the ν(OH) region for the supports evacuated at 573 K. (a) CBV-780; (b) CBV-760; (c) CBV-740; (d) CBV-500; (e) S5A.

feature the well-known bands of bridged hydroxyls at 3630 (HF) and 3565 cm^{-1} (LF), and a sharp band near 3640 cm^{-1} arising from silanols. An entirely different spectrum is found for CBV-500. The weak Si–OH band indicates that this zeolite has not been acid treated; the main feature, however, is a broad absorption between 3680 and 3500 cm^{-1}. Such a signal indicates the presence of an extraframework phase containing Al. The maximum at 3602 cm^{-1} has been previously ascribed to strongly acidic HF hydroxyls perturbed by extraframework species (38). Similarly, the maximum at 3530 cm^{-1} may correspond to perturbed LF/OH, and that at 3667 cm^{-1} to OH groups probably occurring in an amorphous phase containing Al. Finally the spectrum of silica–alumina S5A is much simpler, with a sharp silanol band at 3746 cm^{-1} and a broad signal of associated OH extending down to 3400 cm^{-1}, with a shoulder at 3620 cm^{-1}.

In the IR spectra recorded after adsorption of pyridine, the band at 1545 cm^{-1} is characteristic for pyridinium ions PyH^+, and that at 1455 cm^{-1} reveals coordinated pyridine (LPy). The densities of Brønsted (Br) and Lewis (L) sites can be deduced from their integrated intensities. Results obtained with all supports and with some metal-containing catalysts appear in Table 4. As many more Br and L sites are detected on zeolite CBV-500 than on any other support, the acid sites of this material are likely to be connected with the extraframework amorphous phase. Within the zeolite series, the density of sites regularly decreases with increasing steaming severity, while the framework Si/Al ratio increases. In zeolites CBV-780, -760, and -740, the HF/OH and LF/OH bands disappear upon adsorption of pyridine. However, the decrease of the OH bands cannot account for all of the Brønsted sites deduced from the intensity of the PyH^+. Thus a small part of Brønsted sites in these three zeolites could also belong to the extraframework phase, which contains most of the L sites.

TABLE 4

Numbers of PyH^+ and LPy Detected by IR after Desorption of Pyridine at 393 K

Support	Metal	Si/Al_{fram}[a]	$n(PyH^+)$ ($\mu mol \cdot g^{-1}$)	n(LPy) ($\mu mol \cdot g^{-1}$)	TOF at 393 K (h^{-1})
CBV-780	—	68	68	15	
CBV-780	PtP_{aml}	68	62	15	3800
CBV-760	—	52	96	60	
CBV-740	—	30	131	86	
CBV-740	$PtPd_{Cl}$	30	107	90	2700
CBV-500	—	n.m.	699	220	
S5A	—	—	48	274	
S5A	$PtPd_{am}$	—	44	253	2800
I_1	PtPd	—	45	397	2100
I_2	PtPd	—	56	185	1100
I_3	PtPd	—	58	330	600

[a] Atomic ratio of Si/Al in the zeolite framework, as measured by NMR.

The site densities found on the silica–alumina carrier are intermediate between those on CBV-500 and the other zeolites. The high number of L sites is expected, and the bridged hydroxyls responsible for the protonation of pyridine are obviously more acidic than the silanols, as shown by the persistence of the PyH^+ band upon evacuation. The data in Table 4 further show that the site densities measured on the supports are not substantially changed on loading of the metal, whatever the precursor.

The catalytic activity in hydrogenation (without S) depends heavily on the metal, but the relationship with the density of acid sites on the support is not obvious. Variations in activity are generally smaller than in site numbers, as determined with pyridine. Indeed the activity enhancement brought by the metal–support interaction may be a function of the number as well as the strength of the acid sites. It is interesting that the PtPd catalysts supported on CBV-740 and ASA exhibit similar activities although they feature rather different types of acidity, with a majority of Br sites on the zeolite and of L sites on ASA. The only clear conclusion concerns the catalysts based on CBV-500 which never reached a stable level of activity. For these, self-poisoning is likely a result of the enhanced acidity observed.

Acidity of the Supports: Adsorption of CO

The CO probe is less basic than pyridine and interacts with surface hydroxyl groups mainly through H-bonding, involving rather low energies of adsorption. Thus, studies on acidity by means of CO are better performed at low temperatures, ca. 100 K, where high degrees of coverage may be achieved. Furthermore, CO also interacts with the metal, which may perturb the spectra in the ν(CO) region. Thus the CO probe was used with the bare supports. Indeed it was checked that introduction of the metal ions followed by reduction did not change the number and strength of the acid sites.

Changes occurring in the ν(OH) and ν(CO) regions of the IR spectra are of interest. When CO is adsorbed at 100 K over zeolites CBV-780, -760, and -740, the LF/OH band at 3565 cm^{-1} remains unchanged, in agreement with a previous report (39), but the HF/OH band at 3630 cm^{-1} disappears progressively, while a broader signal develops at about 3280 cm^{-1}. This new vibration is ascribed to a downward shift of the HF/OH band due to the bonding with CO, as highlighted by the difference spectra (Fig. 5). The shifts $|\Delta\nu(OH)|$ of the HF/OH are listed in Table 5 for the whole series of zeolites. As $|\Delta\nu(OH)|$ increases with the acid strength of the hydroxyl (40), the HF/OH groups turn out to have comparable acidities over CBV-780, -760, and -740. From the intensity loss of the initial band at 3630 cm^{-1}, the densities of HF hydroxyls could be evaluated. They are listed as n_1(HF) in Table 5. However the very high shift (372 cm^{-1}) observed on zeolite CBV-500 indicates that this

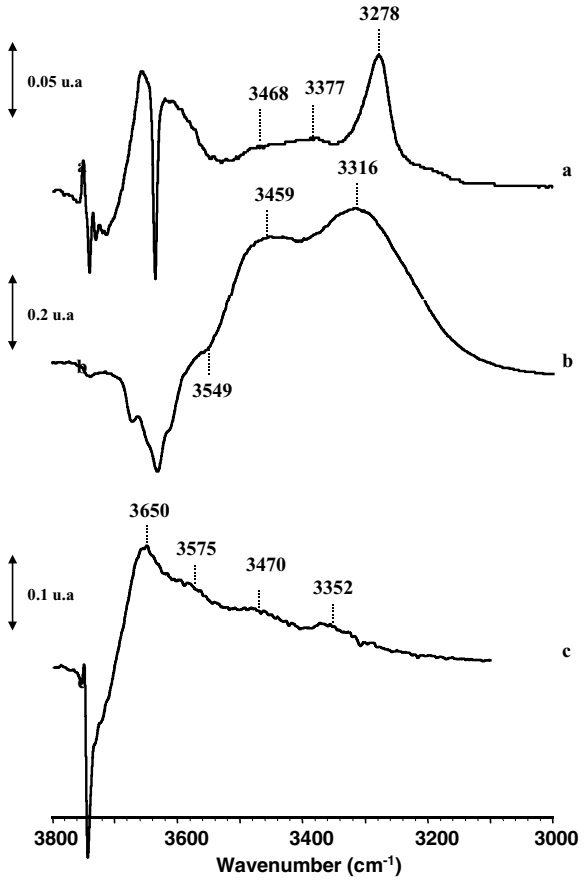

FIG. 5. Difference spectra of hydroxyls in the 3550- to 3300-cm^{-1} region after adsorption of 800 $\mu mol \cdot g^{-1}$ CO at 100 K (spectra of the bare support have been subtracted). (a) CBV-780; (b) CBV-500; (c) ASA.

particular zeolite carries sites with enhanced acidity (38). Even more acidic sites, with $|\Delta\nu(OH)| = 414$ cm^{-1}, may be found over zeolite CBV-740, but their amount is quite small. The Si–OH bands also lose intensity on CO adsorption, while a broad band appears between 3600 and 3700 cm^{-1} (expected $|\Delta\nu(OH)| = 90$ cm^{-1}).

TABLE 5

Interaction of CO with Hydroxyl Groups at 100 K: Shifts $\Delta\nu$(OH) and $\Delta\nu$(CO)

	HF/OH			ASA/OH	
Support	$-\Delta\nu$(OH) (cm^{-1})	n_1 ($\mu mol \cdot g^{-1}$)	n_2 ($\mu mol \cdot g^{-1}$)	$\Delta\nu$(CO) (cm^{-1})	n_2 ($\mu mol \cdot g^{-1}$)
CBV-780	357	25	23	33–26	8
CBV-760	354	32	30	33–26	22
CBV-740	357–414	43	44	33–26	32
CBV-500	314–372	n.m.	171	26	553
S5A	—	—	—	26	82

Note. Numbers of HF and ASA hydroxyls deduced from the intensities of the ν(OH) band (n_1) or of the ν(CO) bands (n_2).

Moreover the difference spectra recorded on stepwise adsorption of CO over zeolites CBV-780, -760, and -740 feature new broad bands with low intensity at 3377 and 3468 cm^{-1}. These bands are thought to arise from an interaction between CO and particular hydroxyls which could not be detected in the 3700- to 3730-cm^{-1} zone of the direct spectra. Their disappearance on CO adsorption is evidenced by negative peaks appearing at 3712, 3719, and 3730 cm^{-1} in the difference spectra. By analogy with silica–alumina, these hydroxyls, noted ASA/OH, likely occur in the extraframework phase (41). The shifts $|\Delta\nu(OH)|$ could not be measured accurately, but their extent means that these hydroxyls do not interact with CO as strongly as the HF/OH. Similar bands characteristic for ASA hydroxyls bound to CO constitute the main feature of the spectra recorded over zeolite CBV-500 and silica–alumina S5A (Fig. 5).

Examination of the spectra in the ν(CO) region brings more information. The band of gaseous CO at 2142 cm^{-1} is shifted to higher frequencies due to interaction of CO with hydroxyls, and the size of the shift, $\Delta\nu$(CO), increases with the acidity of the proton. CO may further interact with Lewis sites. Figure 6 shows the spectra recorded over supports CBV-780 and S5A. Several components may be distinguished in the complex ν(CO) signal. Apart from the band at 2142 cm^{-1} corresponding to quasiliquid CO, several bound species could be identified by comparison with the evolution in the ν(CO) region. In zeolite CBV-780, for instance, CO appears to be bonded to four kinds of protons: HF/OH ($\nu_{CO} = 2179$ cm^{-1}), two types of ASA/OH (2176 and 2169 cm^{-1}), and silanol groups (2157 cm^{-1}, with a 2132 satellite due to ^{13}CO). The same four species are detected over zeolites CBV-760 and -740, but interaction with the HF sites could not be measured over CBV-500. For the ASA support, the main band arises from CO bound to silanols, but the signal at 2172 cm^{-1} reveals hydroxyls with an acidity intermediate between the HF/OH and the silanols. The number of L-bonded CO is highest on this support.

The shifts $\Delta\nu$(CO) corresponding to the hydroxyls on all supports are presented in Table 5. Thus the acid strength of hydroxyl groups increases in the order SiOH $\ll$ ASA $<$ HF, as expected.

Densities of hydroxyls can be deduced from the amounts of CO implied in the bands at 2180 and 2176–2169 cm^{-1}. They are noted n_2 in Table 5. The numbers n_2 of HF/OH detected over zeolites CBV-780, -760, and -740 agree with those (n_1) previously deduced from the decrease of the ν(OH) band. Furthermore the CO probe allows determination of the densities of ASA/OH which could not be reached through the OH bands. According to Table 5, the three Si-rich zeolites feature less ASA than HF hydroxyls. A very high density of ASA/OH is found with CBV-500, although it may be slightly overestimated due to interference with LF/OH. The density of ASA/OH measured on S5A lies

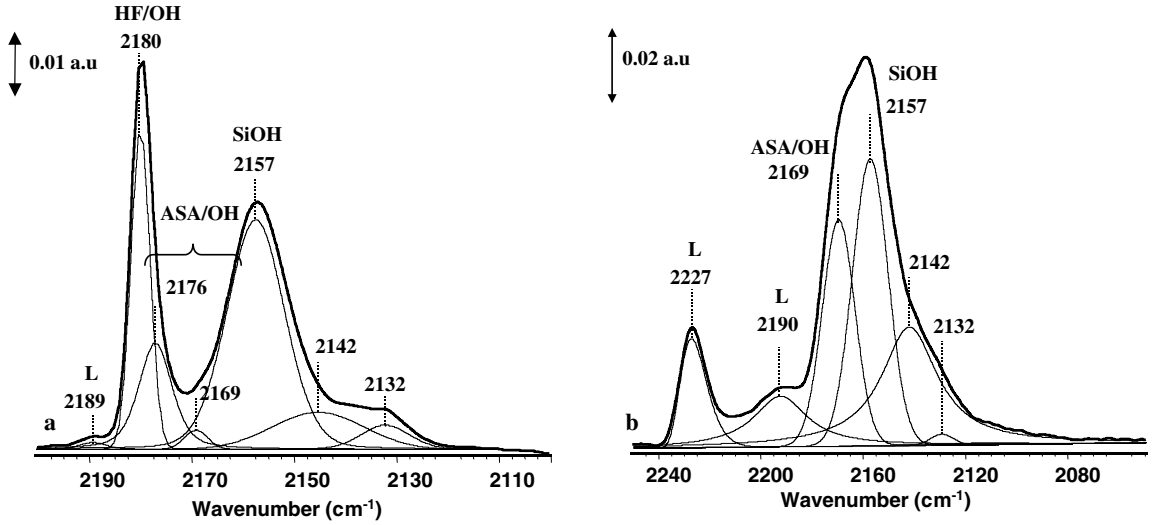

FIG. 6. Difference IR spectra in the ν(CO) region after adsorption of 800 μmol · g^{-1} CO at 100 K. (a) CVB-780; (b) ASA.

between that on CBV-500 and the other zeolites. The sum of (HF + ASA) hydroxyls does not vary much for all the supports, except for CBV-500, which appears very acidic. It is interesting that the sum (HF + ASA) deduced from CO adsorption at 100 K stays inferior to the number of PyH^+ detected at 393 K (Table 4).

Thus, the CO probe indicates that the more acidic protons have comparable strength on all supports. The acid strength may be the most important factor of the metal–support interaction since, as already pointed out, the rates of hydrogenation for a given metal in the absence of sulfur do not vary as much as the site densities. In the case of CBV-500, the relatively few HF hydroxyls are not as strongly acidic as on the other zeolites, as shown by their moderate shift (314 cm^{-1}) on interaction with CO. However, the appearance of a band of perturbed OH at 3258 cm^{-1} at low CO coverage suggests the presence of hydroxyls with enhanced acidity, responsible for deactivation by coke (42). Such sites are also present, albeit in smaller number, on CBV-740, explaining why the corresponding PtPd catalyst is less active than those using the CBV-780 or -760 supports. Therefore, an enhanced acid strength may be detrimental to activity.

Hydrogenation of Toluene in the Presence of Sulfur

The influence of H_2S on hydrogenation was studied with a toluene feed containing 200 ppm S introduced as DMDS. Although the space–time W/F was higher than without sulfur, reaction temperatures had to be raised by ca. 50 K in order to reach comparable conversions at the same $P(H_2) = 3$ MPa. Again methylcyclohexane was the only product. Measurements were performed with random temperature changes up to 503 K; conversions after 2–3 h on stream were quite reproducible and stable, showing the reversibility of sulfur poisoning. Conversions measured at constant flow rate over catalysts with the CBV-780 support are plotted versus temperature in Fig. 7. The results could be interpreted with the same rate law as before, with again (bP_0) values close to 10. Thus the toluene hydrogenation rate is nearly zero order in toluene pressure, in agreement with previous findings (43).

The initial rates, denoted r_S, and the apparent activation energies E_a are listed in Table 6. They differ from the results in the absence of sulfur. For catalysts supported on CBV-780, the results displayed in Fig. 7 suggest that two regimes

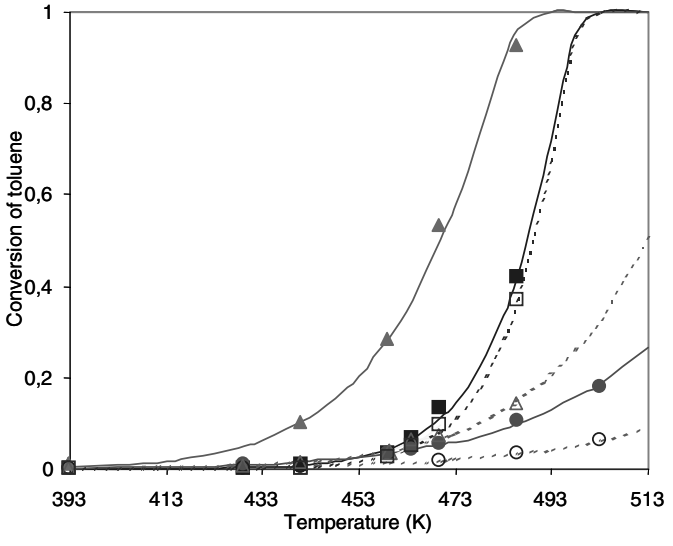

FIG. 7. Hydrogenation of toluene over catalysts supported on CBV-780: conversion versus temperature at $W/F = 0.022$ kg h mol^{-1}; $P(H_2) = 3$ MPa; P_0(tol) = 24 kPa; 200 ppm sulfur. (Solid lines) am precursors: ■, Pt (0.3%); ●, Pd (0.5%); ▲, Pt (0.3%) + Pd (0.5%). (Dashed lines) Cl precursors: □, Pt (0.3%); ○, Pd (0.5%); △, Pt (0.3%) + Pd (0.5%).

TABLE 6

Hydrogenation of Toluene in the Presence of Sulfur: Initial Rates and Sulfur Tolerance at 393 and 473 K

Support	Metal	r_S at 393 K (mol h^{-1} kg^{-1})	S tolerance at 393 K (r_S/r_0)	E_a (kJ mol^{-1})	r_S at 473 K (mol h^{-1} kg^{-1})	S tolerance at 473 K (r_S/r_0)
CBV-780	Pt_{am}	0.0017	0.000015	160	6.6	0.0088
	Pd_{am}	0.053	0.0023	76	2.7	0.0043
	$PtPd_{am}$	0.19	0.0043	96	27.5	0.032
	Pt_{Cl}	0.00046	0.000012	180	5.1	0.020
	Pd_{Cl}	0.017	0.0011	76	0.87	0.0021
	$PtPd_{Cl}$	0.026	0.00065	96	3.6	0.014
CBV-760	$PtPd_{am}$	0.18	0.004	102	34.4	0.113
CBV-740	$PtPd_{am}$	0.22	0.0069	81	14.2	0.017
	$PtPd_{Cl}$	0.17	0.0056	98	26.9	0.055
CBV-500	$PtPd_{am}$	0.16	0.027	78	8.9	0.036
ASA	Pt_{am}	0.011	0.0003	135	11.4	0.012
	Pd_{am}	0.016	0.0006	85	13	0.016
	$PtPd_{am}$	0.41	0.016	80	25.6	0.050
	Pt_{Cl}	0.003	0.00029	131	2.6	0.0054
	Pd_{Cl}	0.029	0.0027	93	3.6	0.0112
	$PtPd_{Cl}$	0.025	0.0017	77	1.3	0.0024
I_1	PtPd	0.066	0.0026	107	17.2	0.060
I_2	PtPd	0.052	0.0022	89	5.2	0.025
I_3	PtPd	0.05	0.0037	83	3.7	0.009

Note. Measurements performed at $P(H_2) = 3$ MPa and $P_0(Tol) = 24$ kPa.

need to be distinguished. At temperatures under 433 K, i.e., at high sulfur coverage, the PtPd catalysts are the most active, with the Pt catalysts becoming less active the Pd ones. Table 6 also shows the values of the sulfur tolerance, defined as the ratio between hydrogenation rates with and without sulfur. For the Pt catalysts supported on CBV-780, this ratio is found to be as low as 10^{-5} at 393 K, showing that Pt is extremely poisoned in the low-temperature region. Poisoning of Pd and PtPd is not so severe with tolerance ratios around 10^{-3}. Concerning the influence of the precursor, the Pt_{am} catalyst turn out to be more active than its Pt_{Cl} analog, although both exhibit equivalent sulfur tolerance. Similarly, the Pd and PtPd catalysts made with the am precursors are more active, but more sulfur-tolerant than those made with the Cl precursors (Table 6).

Poisoning by sulfur leads to an increase in E_a for all metals. The variation is particularly important with Pt, as E_a goes from 36 to 160–180 kJ mol^{-1}. It is more moderate for PtPd (from 36–57 to 96 kJ mol^{-1}) and relatively small for Pd (from 64 to 76). As a result, the difference in activity between the Pt and PtPd catalysts narrows at higher temperature ($T > 453$ K) due to increased sulfur desorption. According to Table 6, the initial rates per unit catalyst mass measured at 473 K vary in the order PtPd > Pt > Pd.

The sulfur tolerance of all metals at 473 K appears also higher than at 393 K, although the smallest value occurs with Pt. Metal accessibilities in the presence of sulfur are unknown, so that turnover frequencies cannot be determined. However quasiturnover frequencies (QTOF) based on the total metal content may be derived from the rates at 473 K. Then, in the high-temperature region, the order of activities per mole of metal appears to be PtPd ≈ Pt > Pd. Again the am catalysts are more active than the Cl ones (Table 6), and their sulfur tolerance is improved, except for Pt.

The influence of the zeolite treatment on catalytic activity was examined in the case of the bimetallic PtPd catalysts only. In the low-temperature region, the initial rates r_S are found to be rather similar for the $PtPd_{am}$ catalysts based on the four zeolites (Table 6), contrary to what was observed in the absence of sulfur. The order of activities differs somewhat, the support CBV-740 now appearing superior to CBV-780. Therefore, the sulfur tolerance depends markedly on the zeolite treatment, and catalysts with the most acidic supports (CBV-740 and CBV-500) display better S resistance than the two other samples. The rates recorded at 473 K vary slightly more than those at 393 K, but in any case sulfur tolerance increases with temperature, as for the CBV-780 catalyst. The influence of the metal precursor was studied with PtPd catalysts using two typical zeolite supports. The behavior is rather contrasted: while the am precursor appears superior for CBV-780, the Cl precursor affords activity much higher than the sample supported on CBV-740 (Table 6). In fact, the $PtPd_{Cl}$/CBV-740 catalyst presents the highest activity and S tolerance at 473 K.

Silica–alumina was then compared to the zeolite supports. At low temperature, catalysts based on S5A present

higher activity and S tolerance than their zeolite analogs, and the improvement is particularly important for the monometallic catalysts containing platinum (Table 6). At high temperature, however, the differences for a given metal are less important. Again, the metal precursor has some influence on the behavior of the S5A catalysts: the samples originating from the am precursors, especially those containing PtPd, appear distinctly more active and more sulfur tolerant than those from the Cl precursors. Thus, the precursor effect observed with S5A is similar to that with CBV-780.

The PtPd industrial catalysts were also tested for toluene hydrogenation in the presence of sulfur. As seen in Table 6, their activities at 393 K are nearly identical and generally inferior to those of our laboratory-made catalysts. The activation energies and sulfur tolerance appear comparable for both series of PtPd catalysts. However, the E_a values differ somewhat between I_1, I_2, and I_3, and their activities at 473 K are more contrasted, with sample I_1 becoming most active.

DISCUSSION

The influence of the metal structure on the activity for toluene hydrogenation will be discussed by considering first the results obtained in the absence of sulfur. Activation energies (E_a) measured on the unpoisoned catalysts were generally found in the range 50–65 kJ mol^{-1}, thus largely independent of the metal and of the support, zeolite, or silica–alumina. Such E_a values agree well with those reported by Vannice and co-workers for monometallic Pt or Pd catalysts (13, 14). However, for two of our Pt catalysts supported on CBV-780 and CBV-760, much lower values were found ($E_a = 36$ kJ mol^{-1}). These may have been slightly underestimated due to diffusional limitations occurring with these particularly active samples. Besides, the data on monometallic catalysts serve only as a basis for comparison with the PtPd samples.

The rate of toluene hydogenation also depends on the acidity of the support. The effect is currently explained by an additional activity linked either to the metal–support interfacial region (14) or to a decrease in electron density of the metal (33, 44). In this work, the mono- and bimetallic catalysts supported on CBV-780 and -760 were found to be more active than those supported on S5A. As the surface of silica–alumina contains more acidic sites than these highly dealuminated zeolites, a purely electronic effect does not appear to be the sole parameter responsible for the differences observed. In addition, the rather low metal accessibility (20–30%) implies an average diameter of metal particle around 3.5 nm, so that in all catalysts the metal–support interface is rather limited. However in zeolites CBV-780 and -760 most of the metal entities are probably located at the well-developed mesoporous surface, ensuring close proximity with the acidic bridged hydroxyls, and hence yielding a more efficient interface. There is thus an optimal strength of acid sites beyond which coking, and hence deactivation, may occur, as already pointed out for the CBV-500 support.

From the IR spectra of chemisorbed CO, it was inferred that mixed metal particles were formed on the bimetallic PtPd catalysts. The new band appearing at 2095 cm^{-1} (Table 4) is ascribed to CO linearly bonded to Pd atoms perturbed by one, or preferably two, neighboring Pt. The asymmetry of the band suggests that some Pt atoms interacting with Pd neighbors may be involved in linear species. Similarly, the new bridged CO species (band at 1875 cm^{-1}) are thought to occur as Pt–CO–Pd or perhaps $Pd_2(CO)$, where the Pd interacts rather strongly with Pt atoms. The contributions of Pd, Pt, and PtPd alloys to the whole spectrum of the bimetallic catalysts may be deduced from the integrated intensities: they are 0.57, 0.03, and 0.40 respectively. As the atomic composition in the PtPd catalysts is 0.76 Pd + 0.24 Pt, the IR results are consistent with a single alloy phase accommodating all the Pt and Pd. But a polyphase model is also possible, in which almost all the Pt is alloyed with Pd but a sizeable amount of Pd, perhaps 50%, remains as a separate phase.

The turnover frequencies measured in the absence of sulfur with the PtPd catalysts were consistently lower than with the monometallic Pt, but higher than with Pd. This evidences interactions between both metals in the alloy, since the lower metal accessibility measured for the PtPd cannot by itself explain the decrease in activity. An alternative explanation could be based on a simple diluting effect of Pt atoms by Pd, as discussed by Cadenhead and Masse (45) and Leon y Leon and Vannice (46). If we assume that the surface composition is identical to the bulk (i.e., 76 at% Pd and 24 at% Pt), a TOF (1.06 s^{-1}) of the $PtPd_{am}$/CBV-780 can be calculated on the basis of the corresponding monometallic catalysts. This calculated TOF matches the measured value. However, such a calculation appears to be spurious and fails when applied to the other bimetallic catalysts (chlorinated precursors) and, more important, to the catalysts tested in the presence of sulfur. In Refs. (15, 45, 46), however, the authors worked either with unsupported PtAu catalysts or $PdCu/SiO_2$ and $PtPd/Al_2O_3$ catalysts, i.e., catalysts where support acidity was very weak. Therefore, the aromatic molecule was most probably adsorbed on the metallic phase, while on the catalysts of this study, the adsorption is believed to take place on the acidic sites of the support located near the interface with the metallic particles (44, 47). It is therefore more likely that an electronic interaction, rather than a simple dilution effect, is responsible for the activity decrease observed on the PtPd catalysts tested in the absence of sulfur.

When measuring the rate of hydrogenation with the H_2S poison, the flow rates of toluene and DMDS were such that every metal atom in the catalyst was contacted with

one S atom within the first 2 h on stream. Thus the sulfur coverage was quasiuniform throughout the catalyst bed. According to the reaction rates at 393 K (high sulfur coverage), the PtPd catalysts appear much superior to any of the monometallic samples, showing that metal–metal interactions in the alloy effectively prevents the adsorption of sulfur (48, 49). Moreover, the influence of the support acidity on the hydrogenation activity of the PtPd catalysts is not as pronounced as without sulfur. For instance, the S5A support is now more effective than any of the zeolites. Furthermore, the CBV-500 appears nearly as active as the other zeolites, probably because the formation of coke observed in the sulfur-free case did not occur in the presence of H_2S. Besides, the am precursor generally leads to more-efficient catalysts, and this cannot be easily interpreted as a dispersion effect. Yasuda and Yoshimura reached a similar conclusion in a study of tetraline–dibenzothiophene conversion on PtPd on various zeolites (7). On less acidic supports like Al_2O_3, the electronic interactions are also claimed to be the cause of sulfur resistance of PtPd catalysts in the dearomatization of a straight run distillate diesel (containing basic nitrogen compounds). Similarly, other authors (6, 50) conclude that the "alloying" effect explains the sulfur resistance of PtPd-based catalysts in the transformation of various S-containing feeds. Relatively low hydrogenation rates are measured at 393 K on the three industrial catalysts: catalysts I_1, I_2, and I_3 behave like catalysts made with the Cl precursor, in the presence as well as in the absence of sulfur.

In the pattern of activities at 473 K (low S coverage), the alloying effect is still important. Thus, the PtPd appears superior to the monometallic catalysts, although the Pt catalysts regain some activity. As in the sulfur-free case, the effect of support acidity is important, as the activity of the PtPd catalysts varies with the support in the following order: CBV-760 > CBV-780 > S5A > CBV-740 > CBV-500. Again the am precursor appears better than the Cl, although according to some authors (51, 52), catalysts containing residual chlorine achieve a better S tolerance. This may explain the striking anomaly observed with our catalysts based on CBV-740, as the $PtPd_{Cl}$ catalyst using this support is much more active than the $PtPd_{am}$.

An alternative explanation could be based on the number of (bi)metallic particles available for catalysis. If one assumes that in the absence of sulfur, there is a strong Pd segregation on the metallic surface, together with an average particle size of

- 4 nm (2.3×10^{15} particles) on the Pt/CBV-780,
- 7 nm (4.2×10^{15} particles) on the PtPd/CBV-780,
- 11 nm (6.8×10^{14} particles) on the Pd/CBV-780,

the activity of the $PtPd_{am}$/CBV-780 should be much higher than the Pd_{am}/CBV-780. This is not the case; in fact the TOF are equivalent (Table 1). On the sulfur-containing catalysts, it becomes more difficult to measure the particle size by adsorption techniques and it is reported that the presence of sulfur induces sintering (53, 54). However, even if one assumes no increase in particle size for the sulfur-containing catalysts, a relation between the number of metallic particle and catalytic activity is obtained only at high temperature (low coverage) on the catalyst originating from the ammoniated precursor.

In conclusion, the behavior of the bimetallic catalysts in the presence of H_2S strongly depends on the reaction temperature, which influences the sulfur coverage of the bimetallic particles. Very strong poisoning is noted at 393 K, where the rate of hydrogenation is reduced by about 10^3, but some activity is recovered at 473 K (factor of 10^2). Similar effects indeed occur with other sulfur compounds, but the temperature at which poisoning is relieved depends on the particular compound. The type of catalyst (acidity requirement of the support and alloying effect) which is more suitable in a given process should vary with the S-containing molecule, and hence with the temperature. These catalytic systems appear quite complex to study, but the various parameters involved allow a great degree of flexibility in the design of catalysts tailored to specific feedstocks (aromatics, sulfur, and basic nitrogen levels) and operating conditions (T, P). Further work is needed, for instance, on (model) feeds spiked with basic nitrogen compounds, in order to assess the loss incurred in the sulfur tolerance of various catalysts.

CONCLUSION

A family of laboratory-prepared zeolite and an amorphous silica–alumina Pt and/or Pd hydrogenation catalysts were prepared by using various metallic precursors. The levels of metals were similar to those encountered in industrial catalysts. The effect of support acidity (number, type, density) was carefully monitored by FT-IR spectroscopy of the bare surface as well with the help of probe molecules (CO and pyridine). The state of the metals (alloying, accessibility, electronic effects) was monitored by CO adsorption followed by FT-IR spectroscopy. The toluene hydrogenating activity of the resulting catalysts was measured in the absence and in the presence of 200 ppm of sulfur. The catalytic results were analyzed using a zero-order law in toluene. Activation energies for the reaction show a marked increase in the presence of sulfur. The relative effects of the various facets of the acidity and the metallic phase were discussed and a picture of two reaction regimes emerged in the presence of sulfur:

- at low sulfur coverage (high temperature), the determining factor is the presence of PtPd alloying.
- at high sulfur coverage (low temperature), the determining factor is the support acidity.

Three industrial catalysts were compared with the laboratory-made catalysts and their performance was in line with the model systems prepared in our laboratory.

Our approach of in-depth characterization of the acidic and metallic functions by combined spectroscopic and catalytic techniques furthers the knowledge required for the rational design of dedicated catalysts.

ACKNOWLEDGMENTS

One of us (K.T.) thanks the Ministère de la Recherche et de Technologie (France) for a Dr. Sc. grant. Comments and suggestions from Dr. P. Moureaux (Shell Global Solutions, France) were greatly appreciated.

REFERENCES

1. Stanislaus, A., and Cooper, B. H., *Catal. Rev.–Sci. Eng.* **36**(1), 75 (1994).
2. Cooper, B. H., and Donnis, B. B., *Appl. Catal. A* **137**, 203 (1996).
3. Didillon, B., Lynch, J., Guillon, E., and Uzio, D., *in* "Proc. 4th European Cong. Catal. Today, Rimini, Italy," p. 31. Tipolito Maraschi, Milan, (1999).
4. Simon, L. J., van Ommen, J. G., Jentys, A., and Lercher, J. A., *J. Catal.* **201**, 60 (2001).
5. Fujikawa, T., Tsuji, K., Mizuguchi, H., Godo, H., Idei, K., and Usui, K., *Catal. Lett.* **63**, 27 (1999).
6. Navarro, R. M., Pawelec, B., Trejo, J. M., Mariscal, R., and Fierro, J. L. G., *J. Catal.* **189**, 184 (2000).
7. Yasuda, H., and Yoshimura, Y., *Catal. Lett.* **46**, 43 (1997).
8. Minderhoud, J. K., and Lucien, J. P., European Patent Appl. 0 303 332, Shell IRM (1988).
9. Lucien, J. P., and Thielemans, G. L., European Patent 0 512 652, Shell IRM (November 11, 1992).
10. Cooper, B. H., Sogaard Andersen, P., and Hannerup, P. N., Spring. Nat. Meet., AIche, Paper 54A (April 1994).
11. Binet, C., Jadi, A., and Lavalley, J. C., *J. Chim. Phys.* **86**, 451 (1989).
12. Tran Mahn, T., Massardier, J., Gallezot, P., and Imelik, B., *Stud. Surf. Sci. Catal.* **11**, 141 (1982).
13. Rahaman, M. V., and Vannice, M. A., *J. Catal.* **127**, 251 (1991).
14. Lin, S. D., and Vannice, M. A., *J. Catal.* **143**, 554 (1993).
15. Rousset, J. L., Stieveno, L., Cadete Santos Aires, F. J., Geantet, C., Renouprez, A. J., and Pellarin, M., *J. Catal.* **197**, 335 (2001).
16. Samanos, B., Boutry, P., and Montarnal, R., *C. R. Acad. Sci.* **274**, 575 (1972).
17. Gelin, P., Siedle, A., and Yates, J., *J. Phys. Chem.* **88**, 2978 (1984).
18. Sheu, L.-L., Karpinski, Z., and Sachtler, W. H., *J. Phys. Chem.* **93**, 4890 (1989).
19. Stakheev, A. Yu., Shpiro, E. S., Tkachenko, O. P., Jaeger, N. I., and Schulz-Ekloff, G., *J. Catal.* **169**, 382 (1997).
20. Hicks, R., Yen, Q.-J., and Bell, A., *J. Catal.* **89**, 498 (1984).
21. Rieck, J., and Bell, A., *J. Catal.* **103**, 46 (1987).
22. Joyal, C., and Butt, J., *J. Chem. Soc. Faraday Trans. 1* **83**, 2757 (1987).
23. Lepage, J. F., *in* "Applied Heterogeneous Catalysis," p. 368. Technip, Paris, 1987.
24. Blomsma, E., Martens, J. A., and Jacobs, P. A., *J. Catal.* **165**, 241 (1997).
25. Tran Mahn T., Candy, J.-P., Gallezot, P., Massardier, J., Primet, M., Vedrine, J. C., and Imelik, B., *J. Catal.* **79**, 396 (1983).
26. Shepard, N., and Nguyen, T. T., *Adv. Infrared Raman Spectrosc.* **5**, 67 (1978).
27. Greenler, R., Burch, K., Kretzschmar, K., Klauser, R., Bradshaw, A., and Hayden, B. N., *Surf. Sci.* **152**, 338 (1885).
28. Ortega, A., Hoffmann, F., and Bradshaw, A., *Surf. Sci.* **119**, 79 (1982).
29. Rades, T., Borovkov, V. Yu., Kazansky, V. B., Polisset, M., and Fraissard, J., *J. Phys. Chem.* **100**, 16238 (1996).
30. Rades, T., Pak, C., Polisset, M., Ryoo, R., and Fraissard, J., *Catal. Lett.* **29**, 91 (1994).
31. Fiermans, L., De Gryse, R., De Donker, G., Jacobs, P. A., and Martens, J. A., *J. Catal.* **193**, 108 (2000).
32. Lieske, H., Lietz, G., and Spindler, H., *J. Catal.* **81**, 8 (1983).
33. Cosyns, J., Frank, J. P., and Gil, J. M., *C. R. Acad. Sci.* **287**, 85 (1978).
34. Ceckiewicz, S., and Delmon, B., *J. Catal.* **108**, 294 (1987).
35. Pope, C. G., *J. Phys. Chem.* **90**, 835 (1986).
36. Yasuda, H., Sato, T., and Yoshimura, Y., *Catal. Today* **50**, 63 (1999).
37. Reyes, P., Pecchi, G., Morales, M., and Fierro, J. L., *Appl. Catal. A* **163**, 145 (1997).
38. Carvajal, R., Chu, P. J., and Lunsford, J. H., *J. Catal.* **125**, 123 (1990).
39. Kubelkova, L., Beran, S., and Lercher, J. A., *Zeolites* **9**, 539 (1989).
40. Knozinger, H., *in* "Acid-Base Catalysis" (K. Tanabe, H. Hattori, T. Yamaguchi, and T. Tanaka, Eds.), p. 147. Kodansha/Verlag Chemie, Tokyo/Weinheim, 1989.
41. Cairon, O., Chevreau, T., and Lavalley, J. C., *J. Chem. Soc. Faraday Trans.* **94**, 3039 (1998).
42. Joly, S., Saussey, J., and Lavalley, J. C., *J. Mol. Catal.* **86**(1–3), 401 (1994).
43. Lin, T.-B., Jan, C.-A., and Chang, J.-R., *Ind. Eng. Chem. Res.* **34**, 4284 (1995).
44. Lin, S. D., and Vannice, M. A., *J. Catal.* **143**, 563 (1993).
45. Cadenhead, D. A., and Masse, N. G., *J. Phys. Chem.* **70**, 3558 (1966).
46. Leon y Leon, C. A., and Vannice, M. A., *Appl. Catal.* **69**, 305 (1991).
47. Chupin, J., Gnep, N. S., Lacombe, S., and Guisnet, M., *Appl. Catal.* **206**, 43 (2001).
48. Gallezot, P., *Catal. Rev.–Sci. Eng.* **20**(1), 201 (1980).
49. Figoli, N. S., and L'argentiere, P. C., *Catal. Today* **5**, 403 (1989).
50. Lee, J.-K., and Rhee, H.-K., *J. Catal.* **177**, 208 (1998).
51. Apesteguia, C. R., Trevizan, S. M., Garetto, T. F., Plaza, J. F., and Parera, J. M., *React. Kinet. Catal. Lett.* **20**(1–2), 1 (1982).
52. Barbier, J., Marecot, P., Tifouti, L., Guenin, M., Breysse, M., and Frety, R., *Bull. Soc. Chim. Fr.* **49**, 1 (1986).
53. Vaarkamp, M., Miller, J. T., Modica, F. S., Lane, G. S., and Koningsberger, D. C., *J. Catal.* **138**, 675 (1992).
54. Chang, J. R., Chang, S. L., and Lin, T. B., *J. Catal.* **169**, 338 (1997).